RSC Advances

PAPER

Cite this: *RSC Adv.*, 2022, **12**, 25675

A portable colorimetric chemosensing regime for ractopamine in chicken samples using μPCD decorated by silver nanoprisms†

Hossein Navay Baghban, [ab] Mohammad Hasanzadeh, *[cd] Yuqian Liu [a] and Farzad Seidi *[a]

In recent years the use of ractopamine (RAC), originally synthesized for the treatment of respiratory diseases, is on the rise as a dietary supplement in animals. The excessive use of RAC has some adverse effects on human health. Hence, the demand for simple, easy-to-use, and expendable devices for RAC recognition, even in remote areas, is felt more than ever before. This need prompted us to devise a straightforward colorimetric system for RAC recognition based on the etching effect of RAC on AgNPrs. This nanoprobe is a very advanced materials with great optical properties and stability, which could be used unprecedentedly without any combination or reagents for RAC recognition. Considering the needs and advantages, a simple colorimetric chemosensor for the quantification of RAC was designed and applied to a chicken sample. The designed chemosensor was integrated with an optimized microfluidic paper-based colorimetric device (μPCD), creating a suitable tool for the determination of RAC based on a time/color pattern. The analytical metrics for this simple colorimetric chemosensing regime comprise a best colorimetric LLOQ of 100 μM in solution with 10 μM of μPCD, a spectroscopic LLOQ of 10 nM, and a broad linearity range of 0.1–10 000 μM, which are outstanding compared with other colorimetric techniques. The main remarkable features of this study include the first utilization of AgNPrs with high stability and excellent optical properties without any reagent as an optical sensing probe and optimized μPCD toward RAC recognition and the innovative time/color semi-analytical recognition method. Moreover, the prepared portable μPCD modified with AgNPrs could be a prized candidate for commercialization due to the benefits of the low-cost materials used, like paper and paraffin, and the simple instructions for μPCD preparation. This report could be a pioneering work, inspiring simple and effective on-site semi-analytical recognition devices for harmful substances or illegal drugs, which simply consist of a piece of lightweight paper and one drop of the required reagent.

Received 1st August 2022
Accepted 29th August 2022

DOI: 10.1039/d2ra04793d

rsc.li/rsc-advances

1. Introduction

Ractopamine (RAC), a β-adrenergic agonist, has been prescribed to treat respiratory diseases including asthma in mammals.[1,2] Using RAC as a dietary supplement has been shown to help decrease fat levels and stimulate muscle tissue development at the same time in animals.[3] Nevertheless, β-agonists such as RAC aggregate in livestock tissues and may induce acute poisoning in humans, resulting in heart palpitations, tachycardia, anxiety, nausea, fever, and chills, as well as muscle tremors and disorientation.[4–6] The MRL of RAC in animal tissue is 50 μg kg^{-1} in the United States. Nevertheless, RAC is illegal in food-producing animals in the European Union, China, and Thailand, except for therapeutic usage under veterinarian care.[7–9] Diverse analytical techniques for detecting and quantifying RAC residues in feeds and biological samples from animals have been published in an attempt to curb the unlawful use of RAC. The most prevalent are gas chromatography,[10] liquid chromatography,[11] enzyme-linked immunosorbent assays, lateral flow immunoassays,[12–15] and electrochemical bio(sensors).[16–18] However, the majority of the techniques employed need expensive apparatus and complex methodologies, or their commercialization is not easy owing to high prices. Therefore, a simple and cost-effective analytical approach for broad use remains vital. To address this need, colorimetric methods for detecting β-adrenergic agonists with acceptable selectivity and sensitivity standards have gained currency in recent years due to their low cost combined with the

[a]Jiangsu Co-Innovation Center for Efficient Processing and Utilization of Forest Resources and International Innovation Center for Forest Chemicals and Materials, Nanjing Forestry University, Nanjing 210037, China. E-mail: f_seidi@njfu.edu.cn
[b]Food and Drug Safety Research Center, Tabriz University of Medical Sciences, Tabriz, Iran
[c]Pharmaceutical Analysis Research Center, Tabriz University of Medical Sciences, Tabriz, Iran. E-mail: hasanzadehm@tbzmed.ac.ir
[d]Nutrition Research Center, Tabriz University of Medical Sciences, Tabriz, Iran

† Electronic supplementary information (ESI) available. See https://doi.org/10.1039/d2ra04793d

ease of visual inspection.[19–24] On top of these, the commercialization of colorimetric sensors can be more cost-effective than other methods.[25]

Anisotropic noble metal nanoparticles of various forms and sizes have piqued the curiosity of scientists.[26–28] Among them, silver and gold nanoparticles have drawn a lot of attention in recent years, primarily thanks to their chromogenic characteristics and optical properties.[29] To date, various strategies have been used, based on changes in size, shape, and inter-particle distance for designing colorimetric chemosensors based on AgNPs and AuNPs.[20,22,30,31] In this regard, the aggregation–disaggregation approach has some drawbacks, including instability of bonded nanoparticles as well as unwanted effects of interferents in real samples.[32] There are also some compelling reasons for choosing AgNPs over AuNPs. In the first place, the molar extinction coefficient of AgNPs is roughly 100 times larger than that of AuNPs when they are compared at the same size, leading to an improvement in visibility and, subsequently, sensitivity.[33] In the second place, AgNPs are more affordable than AuNPs. Considering these issues, three types of AgNP, namely silver nanoprisms (AgNPrs), silver nanowire (AgNWs), and Ag-Cit NPs, were synthesized in this work and applied for the optical detection of RAC in real samples. According to the obtained colorimetric results, AgNPrs were by far the best candidate to develop an RAC recognition system.

From previous studies, it is obvious that AgNPrs possess plate-like triangle shapes with wonderful electronic, optical and structural features. The LSPR for AgNPrs across visible-NIR regions is robust and any applied changes in vertex form, thickness, or edge length will alter its intensity.[34–38] Based on these facts, AgNPrs have a special place in colorimetric sensors. So far, several sensors and biosensors have been developed by either etching or growth of different analytes onto this nanoprobe.[39–44]

Recently, there has been a lot of interest in the integration of modern sensors on microfluidic substrates.[45] This is mainly because microfluidic systems offer a miniaturized automated environment for the precise analysis of analytes in a micro-scale volume with time and cost efficiency.[46] A microfluidic paper-based colorimetric device (μPCD) is one of the most cost-effective microfluidic systems, which can be readily made with minimal laboratory requirements. Moreover, the instructions for preparing μPCD are straightforward and adjustable. In such systems, the lateral force caused by the nature of the paper will flow any injected solutions across the engulfed channels using hydrophobic materials like paraffin.[47] The last part of this study was devoted to the integration of the proposed colorimetric system into an optimized μPCD modified by AgNPrs for RAC analysis.

In this study, we checked three different kinds of AgNPs, namely AgNPrs, Ag-Cit NPs, and silver nanowire (Ag NWs), for a decent colorimetric response to the existence of RAC. AgNPrs due to their distinct color change were chosen for further investigation. In order to design an RAC colorimetric chemosensor based on AgNPrs and μPCD modified by AgNPrs, several colorimetric and spectroscopic tests were conducted with consideration of reaction time. Notably, two kinds of selectivity test (simple and combinative) with potential interferences were conducted and interpreted in full detail. Finally, an optimized way of producing μPCD for a readily absorbed solution like AgNPRs and a novel method for an approximate assessment of RAC concentration on the basis of a time/color pattern was introduced.

2. Experimental details

2.1. Reagents and materials

Silver nitrate ($AgNO_3$), silver chloride (AgCl), PVP K-30 (polyvinyl pyrrolidone), sodium borohydride ($NaBH_4$, 96%), hydrogen peroxide (H_2O_2, 30 wt%), and tri-sodium citrate ($Na_3C_6H_5O_7$) were purchased from Sigma Aldrich (Canada). Ethylene glycol (EG), methanol, ethanol, cysteine (Cys), aspartic acid (Asp), arginine (Arg), ascorbic acid (VIT C), dopamine (DA), uric acid (UA), and glucose (Glu) were obtained from Merck (Germany). Ractopamine hydrochloride was obtained from TOCRIS (Canada). The chicken was purchased from the local market (Tabriz, Iran).

2.2. Instrumentation

A Shimadzu UV-1800 UV-Vis spectrophotometer with 1 nm resolution was used to measure absorbance. The formation of silver nanoprisms was confirmed by using a transmission electron microscope (TEM, Adelaide, Australia), with a 200 kV voltage supply, and the size distribution and zeta potential of the formed silver nanoprisms were characterized using a Zetasizer Ver. 7.11 (Malvern Instruments Ltd, MAL1032660, England). High-resolution field-emission scanning electron microscopy (FE-SEM; Hitachi-Su8020, Czech Republic) with an operating voltage of 3 kV was used to examine the surface geometry of the silver nanoprisms. A Nanosurf (AG, Liestal, Switzerland) device in tapping mode was used to obtain AFM.

2.3. Photography and colorimetric approach

All of the photographs and videos in this work were taken with a smartphone. Aiming for a universal and error-free colorimetric approach, the hue of the solutions and droplets on μPCD were given an RGB code using Instant-eyedropper software.[48] Then, the given codes were converted to color names using the Colorxs site[49] (Table S1 (see ESI†)).

2.4. Synthesis of silver nanoprisms (AgNPrs), Ag-Cit NPs, and silver nanowires (AgNWs)

All glassware used in the following methods was washed in an HCl/HNO_3 solution, rinsed completely with water, and dried in the air. All of the studies were conducted with double-distilled water.

2.4.1. Ag-Cit NPs. To begin with, 400 mL of $Na_3C_6H_5O_7$ (1.06 mM) solution was mixed with 25 mL of $AgNO_3$ (5 μm) solution and swirled in an ice-water bath. Then, 2.5 mL of a freshly prepared $NaBH_4$ (100 mM) solution was added drop by drop to the mixture. As a result, the transparent solution became pale yellow. The solution was then shaken for around 2 hours in a dark place until a bright golden color appeared. The resulting colloids were then centrifuged at 15 °C for 15 minutes at 6000 rpm.

2.4.2. Silver nanoprisms (AgNPrs). A polyvinylpyrrolidone (PVP) solution (0.06 g PVP in 3 mL) was diluted in 200 mL of water. Then, 4 mL of $AgNO_3$ solution (0.01 M) and 8 mL of trisodium citrate (TCS) solution (75 mM) were added to the solution. Subsequently, 960 mL of H_2O_2 was poured into the mixture and agitated. Finally, 3.2 mL of $NaBH_4$ solution (100 mM), as a reducing agent, was added to the reaction medium to reduce the Ag^+ into Ag(0) in the form of Ag NPrs with vivid yellow coloring of the solution, which changed to bright yellow after a few moments. Ultimately, with 30 minutes of stirring, the color of the colloidal mixture changed to blue. This mixture was stored at 4 °C for future use.

2.4.3. Silver nanowires (AgNWs). First, EG (20 mL) and PVP (0.668 g) were mixed in a flask for 30 minutes at 170 °C. To generate the seeds, 0.05 g of finely sliced silver chloride (AgCl) was added and agitated. After that, 0.22 g of silver nitrate ($AgNO_3$) per 10 mL of EG was added to the prepared solution to develop the nanowires. Heating at 170 °C for 30 minutes completed the growth of NP seeds. After cooling, the mixture was centrifuged for 30 minutes at 6000 rpm in methanol to remove impurities such as PVP and EG.

2.5. Preparing a real sample of chicken flesh

A 2.5 CC microtube was filled with 0.5 g of minced chicken breast flesh. Next, 1 mL of ethanol and 0.5 CC of RAC (0.01 M) were added to the microtube. The prepared mixture was sonicated for 10 minutes and in the next step was centrifuged for 5 minutes at 10 000 rpm. Finally, the supernatant solution was collected with a sampler and the analyte concentration was determined. A control sample was prepared in the same manner, except that distilled water was used instead of the analyte.

2.6. Paper-based microfluidic device fabrication

The paper-based microfluidic device was fabricated in an innovative way to achieve appropriate colorimetric results with a micro-scale of sample in an economical and easy-to-use manner. For this purpose, fiberglass paper and fiberglass paper sunk in molten paraffin were pressed together in the middle of a robust magnet and designed iron stencil which had already been heated up to 160 °C. As a result of simultaneous heating and pressurizing, the untouched hydrophilic zone of the fiberglass paper was surrounded by tissue impregnated with paraffin (hydrophobic area). The hydrophilic area created was a network of a central circle forking off into eight channels that terminated in 8 smaller circles. A scheme, drawn with CorelDRAW software, was used to create the iron stencil with all of the respective dimensions. The prepared μPCD after drying was utilized for colorimetric analyses (Scheme 1).

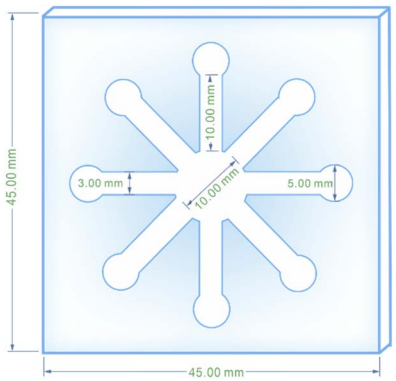

Scheme 1 The pattern of the designed stamp drawn using CorelDRAW software.

2.7. Identifying appropriate AgNPs for RAC detection

Three different AgNPs, namely AgNPrs, Ag-Cit, and AgNWs, were synthesized and introduced to standard 0.01 M RAC solution in a 1 : 1 ratio to produce discrete color changes for analyte recognition. As shown in Fig. 1, for AgNPrs there was a clear color change. As soon as the RAC solution was added to

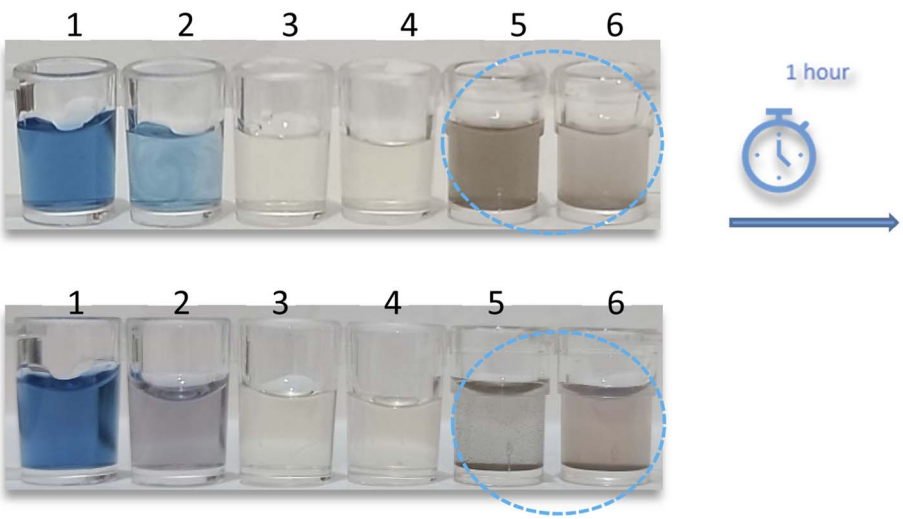

Fig. 1 Photographic images of (1) AgNPrs, (2) AgNPrs + RAC 0.01 M (1 : 1), (3) Ag-Cit, (4) Ag-Cit + RAC 0.01 M (1 : 1), (5) AgNWs, and (6) AgNWs + RAC 0.01 M (1 : 1). The volumes of AgNPs and RAC were 100 μL.

the AgNPrs, its color altered from sea blue to moonstone blue. Interestingly, after one hour (the reaction time was twenty minutes) the color of the mixture had completely changed to taupe gray. The combination of Ag-Cit and RAC aqueous solution showed no color change, while AgNWs after combining with RAC showed a trivial color change. Accordingly, AgNPrs were selected for further examination.

3. Characterization

There are numerous methods for the characterization of nanoparticles that can be selected according to their favorable underlying features. The morphology and size of nanoparticles are two major factors of common interest in this regard. These properties are definable by FE-SEM, TEM, and AFM microscopes. EDS is also an authentic method for determining the elements comprised at the nanoscale. DLS is a common technique to obtain well-rounded knowledge of the size distribution as well as the zeta potential of particles.

In this study, all of these techniques were used for AgNPr characterization. Once again, DLS was used for investigation of the size distribution of AgNPrs after reaction with RAC. In addition to these analytical approaches, colorimetric detection coupled with UV-Vis absorbance quantification were indispensable parts of this study for the characterization of AgNPrs and AgNPrs in the presence of RAC.

3.1. Characterization of AgNPrs

Recorded TEM images (Fig. S1 (see ESI†)) revealed that the synthesized AgNPrs possess a triangular shape. Furthermore, graphs taken by FE-SEM gave fresh insight, confirming the TEM observation. In these images with a field of view of 4.15 μm to 1.04 μm, AgNPrs seemed to be arranged like sunflower seeds with separable particles ranging from 14.22 to 23.97 nm (Fig. S2 (see ESI†)). As a final visualization step, AFM provided three-dimensional images of the topography of the AgNPr particle surface (Fig. S3 (see ESI†)), and confirmed the TEM and FE-SEM graphs. Fig. S3B and C (see ESI†) gave more detailed data on the topographical range of the particles in a 5 μm^2 square, which was consistent with the aforementioned results.

Another required feature for the study of AgNPr properties is their zeta potential. According to one study, synthesized nanoparticles will enjoy decent stability if their zeta potential is either more positive than +30 V or more negative than −30 V.[50] Additionally, a greater zeta potential can reduce the aggregation as well as the growth in size growth of the nanoparticles.[50] Since this figure for synthesized AgNPrs was found to be −67.5 mV (Fig. S4 (see ESI†)), this nanoparticle is considered to have a good condition of stability.

3.2. RAC reaction confirmation with color change, UV-Vis spectra absorption, and DLS

The prepared AgNPr colloidal solution was sea blue. As soon as colorless RAC solution (0.01 M) was added, the color changed to pewter blue. Then after colorless RAC solution (0.01 M) was added, its hue changed to a brighter shade of turquoise. After 20 minutes, the color of the mixture had altered to brick red.

The UV-Vis spectra for AgNPrs, RAC, and AgNPrs after adding RAC (0.01 M) after different time intervals are shown in Fig. 2. For AgNPrs, three LSPR peaks at 335, 450 and 655 nm are related to the out-of-plane quadrupole resonance, the in-plane quadrupole resonance, and the in-plane dipole resonance, respectively, for AgNPrs.[51] Hence, these three absorption bands confirmed the formation of AgNPrs. Upon spiking AgNPr solution with RAC (0.01 M), the intensity of the bands of the solution decreased significantly and a λ shift occurred towards a lower spectrum for the absorption band at 655 nm. The biggest λ shift occurred for this band after 20 minutes at −169 nm, which remained unchanged at 475 nm after 1 hour.

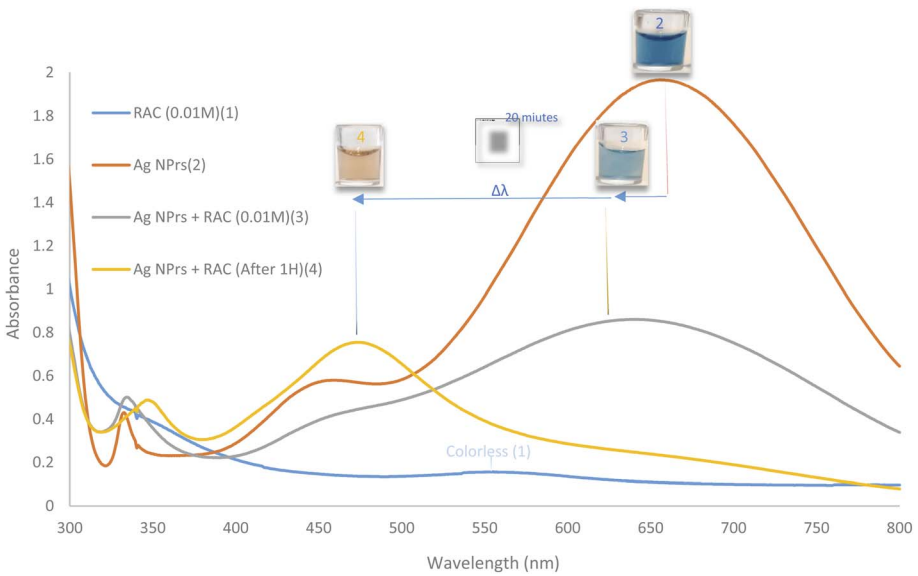

Fig. 2 UV-Vis absorption spectra of RAC (0.01 M), AgNPrs, AgNPrs + RAC (0.01 M), and AgNPrs + RAC (0.01 M) after 1 hour.

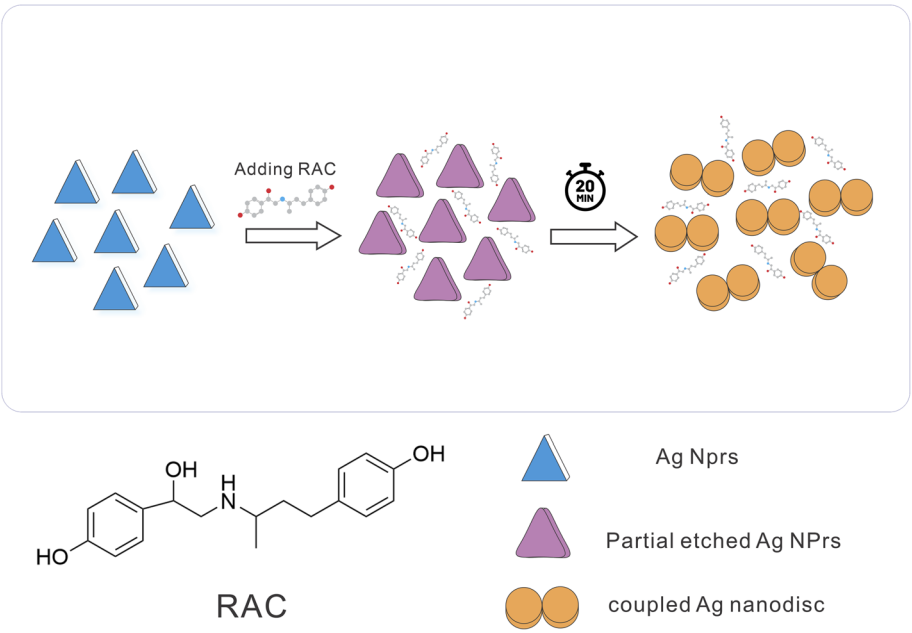

Scheme 2 Two distinct hues produced *via* the etching process of RAC on AgNPrs.

DLS showed a diameter of 0.84 nm for AgNPrs which reduced to 0.71 nm upon the addition of RAC, which was related to the etching effect of RAC on the Ag NPrs vertices. After the complete color change (~20 minutes), the diameter of the AgNPrs reached 1.81 nm (Fig. S5 (see ESI†)). A possible reason is related to the conversion of AgNPrs into disks over long-term etching,[30,52] so that these disks are bundled in multiple batches (Scheme 2).

4. Results and discussion

4.1. Concentration effects of RAC

To study the concentration effect of RAC by colorimetric and spectroscopic methods, various concentrations of RAC (0.01 to 10 000 μM) were prepared in deionized water. Then, AgNPrs were added with a 1 : 1 v/v ratio. These mixtures were photographed immediately, after 30 minutes and after 50 minutes. After 30 minutes had passed, 100–10 000 μM concentrations of RAC had changed the blue color of the AgNPrs to taupe. 20 minutes later, the color of these concentrations had turned to a brighter shade and stabilized on bone color. The results show that the effect of RAC on AgNPrs not only depends on its concentration but that reaction time is also a key factor. Based on this result, the presence down to a minimum concentration of 100 μM of RAC in a standard solution would be easily distinguishable by the naked eye (Fig. 3B).

The second part of this study was allocated to reading the UV-Vis spectra of standard samples 50 minutes after mixing with AgNPrs owing to the fact that their color at this point remained nearly stable. As shown in Fig. 3, RAC with concentrations of 100–10 000 μM has the capability of shifting the spectrum of the absorption band substantially, causing a change in the solution color from dark turquoise to yellowish red. Subsequently, the regression equation of $\lambda = 0.0007C\,(\mathrm{RAC}) + 473.61$ ($R^2 = 0.8959$) was achieved, which confirmed the linear relationship between wavelength and concentration in this concentration range. Furthermore, the absorbance band was in a linear relationship with RAC concentration over the ranges of 0.1–50 μM and 500–10 000 μM with regression equations of $\mathrm{Abs} = -0.003C\,(\mathrm{RAC}) + 1.2262$ ($R^2 = 0.8115$) and $\mathrm{Abs} = -3 \times 10^{-5}\,C\,(\mathrm{RAC}) + 1.2464$ ($R^2 = 0.9123$), respectively. The regression equation $\mathrm{Abs} = -0.0642C\,(\mathrm{RAC}) + 1.2156$ ($R^2 = 0.9377$) was also obtained over the whole concentration range of 0.1–10 000 μM, which confirms the downward trend of the absorption band in relation to the logarithm of RAC concentration. According to the acquired data, the proposed colorimetric assay based on AgNPrs has a linear range and LLOQ of 0.1–10 000 μM and 0.01 μM, respectively.

As shown in Table 1, the analytical values for the proposed system are at an acceptable level compared with previously reported colorimetric systems and, considering the simple preparation of the proposed sensor without the use of a reagent, this colorimetric system can be placed among valuable colorimetric approaches. Notably, the wide linearity range of this system compared with others covers a much greater range of concentration of RAC from nanomolar to millimolar. The first use of chicken as a real sample for RAC analysis is another advantage of this work, because of the vast use of poultry and byproducts across the world.[53]

Table 2 compares the LOD/LLOQ and linear range for RAC detection using colorimetric RAC chemosensory and other reported analytical methods. The linearity range for this system is greater than the others, apart from the electrochemical method. The limit of detection for this colorimetric system and other different methods, apart from the electrochemical method, is in the nanomolar range. Although the LLOQ and linearity in a low

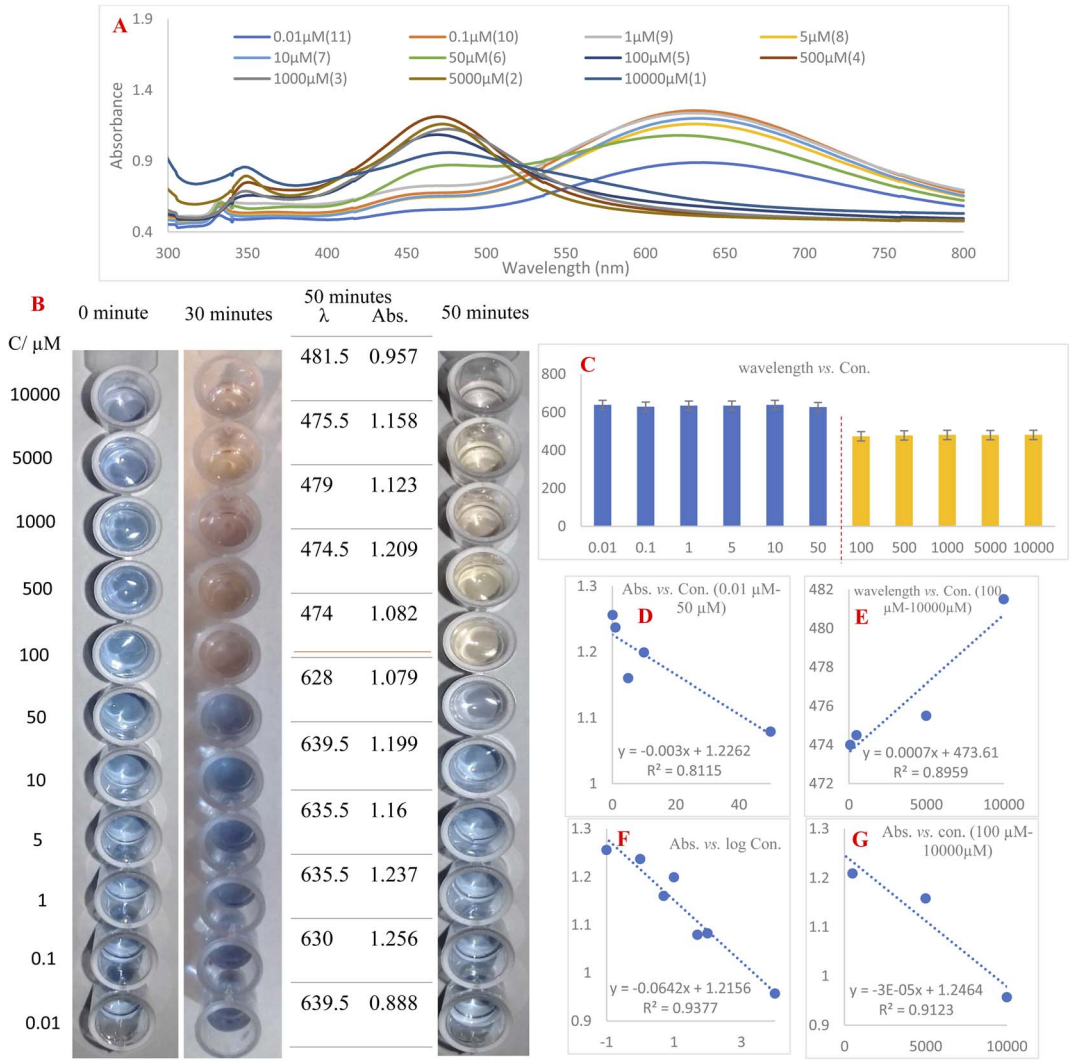

Fig. 3 (A) UV-Vis spectra of different concentrations of RAC with AgNPrs at a 1 : 1 ratio after 50 min. (B) Digital images of AgNPrs spiked with RAC of various concentrations at three different times (the ratio was 1 : 1). (C) The dependency of wavelength on RAC concentration and (D) the calibration curve of peak intensity *versus* RAC concentration from 0.01 μM to 50 μM. (E) A calibration curve of wavelength *versus* RAC concentration from 100 μM to 10 000 μM. (F) A calibration curve of peak intensity *versus* the logarithm of RAC concentration. (G) A calibration curve of peak intensity *versus* RAC concentration from 100 μM to 10 000 μM.

concentration of RAC for the designed colorimetric method are not as good as some of the other mentioned methods, these analytical values are sufficient. (The RAC MRL in animal tissue is 50 μg kg^{-1} in the United States.)[22]

Additionally, colorimetric methods are simple and straightforward and can be done without any sophisticated equipment or professional experts. Moreover, this colorimetric method is capable of RAC recognition with a minimum concentration of

Table 1 A comparison between the proposed colorimetric system and previously reported methods

Reaction system	Matrix	Linear range (ng mL^{-1})	LOD/LLOQ (ng mL^{-1})	Ref.
Fe_3O_4@β-CD PtNPs-PV (immunosensor)	Pork	0.03–8.1	0.01	19
$NaHSO_4$-optimized AuNPs	Pig urine	1000–9000	22.9	20
Sulfanilic acid-modified AuAgNPs	Spiked pork, swine feed, and swine urine	4.5–31.6	1.5	22
PE-Glu-AuNPs	Human urine	0–351	0.344	23
AuNP-based (ELISA)	Urine	2–512	0.35	54
SiW_9Cu_3	—	54 811–131 050	27 897	24
AgNPrs	Chicken	35.13–3 513 500	3.513	This work

Table 2 A brief comparison of various reported analytical methods with the proposed colorimetric system

Analytical method	Matrix	Linear range (ng mL^{-1})	LOD/LLOQ (ng mL^{-1})	Ref.
Capillary electrophoresis	Pig feed, pig urine, and pig liver	96–47 920	86.5	55
Gas chromatography	Feed	10.4–519.96	4.1459	56
Electrochemical	Human plasma	0.00154×10^{-6}–6868	0.00154×10^{-6}	57
ECL	Swine urine	0.026–3.127	0.0087838	9
HPLC	Monkey plasma and swine serum	0.527–41.6	2.0730	58
ELISA	Sheep urine	2–512	0.35	54
Colorimetric	Chicken	35.13–3 513 500	3.513	This work

100 μM in standard samples and 10 μM in modified μPCD based on the etching effect of AgNPrs on RAC without any additional reagent by the naked eye. The above-mentioned electrochemical biosensor indeed has great analytical features, but the miniaturization of this approach needs more costing and study. In addition, it requires a portable electronic device with a power source. Other methods cannot be miniaturized. Since the proposed analytical method does not require any supportive device, unlike the other mentioned techniques, it can be easily miniaturized and developed as an inexpensive on-site recognition device based on a simple color change phenomenon.

4.2. Colorimetric and UV-Vis spectroscopic measurements in a real sample with AgNPrs

The reported colorimetric and spectroscopic approaches were also utilized to detect spiked RAC in chicken extract samples (Fig. S6 (see ESI†)).

Based on the results acquired from the comparison test, different concentrations (100–3330 μM) of spiked RAC in the chicken extract were mixed with AgNPrs in a 1 : 1 v/v ratio. Then they were analyzed by colorimetric and spectroscopic methods. According to the obtained results (Fig. S7 (see ESI†)), concentrations lower than 500 μM could not change the color of the mixture to brighter blue. Evaluating the UV-Vis absorption response showed a linear relationship between the wavelength of the absorption band with the concentration of RAC over the range of 100–700 μM.

4.3. Selectivity analysis

The selectivity of the proposed technique was evaluated by performing the assessment in the presence of other species in real samples. In practice, 0.01 M solutions of cysteine (Cys), aspartic acid (Asp), arginine (Arg), ascorbic acid (VIT C), dopamine (DA), uric acid (UA), and glucose (Glu) in 1 : 1 v/v ratio were mixed with AgNPr solution and the results were compared with an RAC/AgNPrs mixture under the same conditions to detect any resemblance to an RAC effect they may have on AgNPrs (Fig. S8 (see ESI†)). Since the etching effect of RAC and other similar species on AgNPrs depends on reaction time, the time for examination was set to 1 min after mixing the components.

While other mixtures changed the color to a brighter shade of turquoise, the AgNPrs/RAC solution hue transformed to bright purple. Moreover, the UV-Vis spectrum of the AgNPrs/RAC solution showed unique features. In fact, it showed no overlap with other species except for AgNPrs/DA; but the intensity of the AgNPrs/DA peak was around twice as weak as the one for AgNPrs/RAC. The obtained data revealed the high selectivity of AgNPrs toward RAC in the first minute of reaction if the AgNPrs/RAC solution and interferent species/RAC are compared separately.

In the second part, 50 μL of RAC (0.1 mM, the minimum required concentration of RAC for shifting the color of the AgNPrs to bone) was combined with 50 μL of interferential species (0.1 mM). Then, 100 μL of AgNPrs was added to the RAC/interference mixture and photographed after 2 and 30 min. The UV-Vis spectrum was also recorded after 30 min (Fig. 4).

The complete color change to bright purple after 2 min of reaction was just obtained for the RAC/AgNPrs mixture and the color of the (interference/RAC)/AgNPrs mixtures had changed to brighter turquoise. As adding an interference species halved the concentration of RAC, it could be reasonable that the color of the AgNPrs had not changed in other mixtures. Nevertheless, after 30 minutes, the color of (RC/Glu)/AgNPrs, (RAC/Asp)/AgNPrs, and (RAC/Arg)/AgNPrs had turned to bright purple. At that time of reaction, the hue for the RAC/AgNPrs solution had turned yellow. Therefore, Glu, Asp, and Arg have a synergic effect on etching AgNPrs with passing time. Moreover, according to UV-Vis spectrometry, if RAC is the only analyte, it can be readily detected as the absorption of RAC/AgNPrs at the shifted absorbance band was the highest and in the vicinity of the main absorbance band of AgNPrs it was the lowest.

4.4. Stability

The stability of AgNPr colloidal solution was tested for 20 days. As shown in Fig. S9 (see ESI†), the hue of the solution was almost consistent during this period. Importantly, the result obtained from the UV-Vis spectrum does not show any substantial alteration in the three absorption bands. Although the intensity of the absorption bands diminished gradually, this reduction ratio for all three absorption bands was roughly the same without affecting the wavelength position. That is why the color of the solution did not undergo any changes.

4.5. Colorimetric RAC analysis using microfluidic paper

4.5.1. Integration of the colorimetric recognition system with microfluidic paper. To integrate the colorimetric RAC analysis system with microfluidic paper, two kinds of microfluidic papers were prepared and underwent examination. In

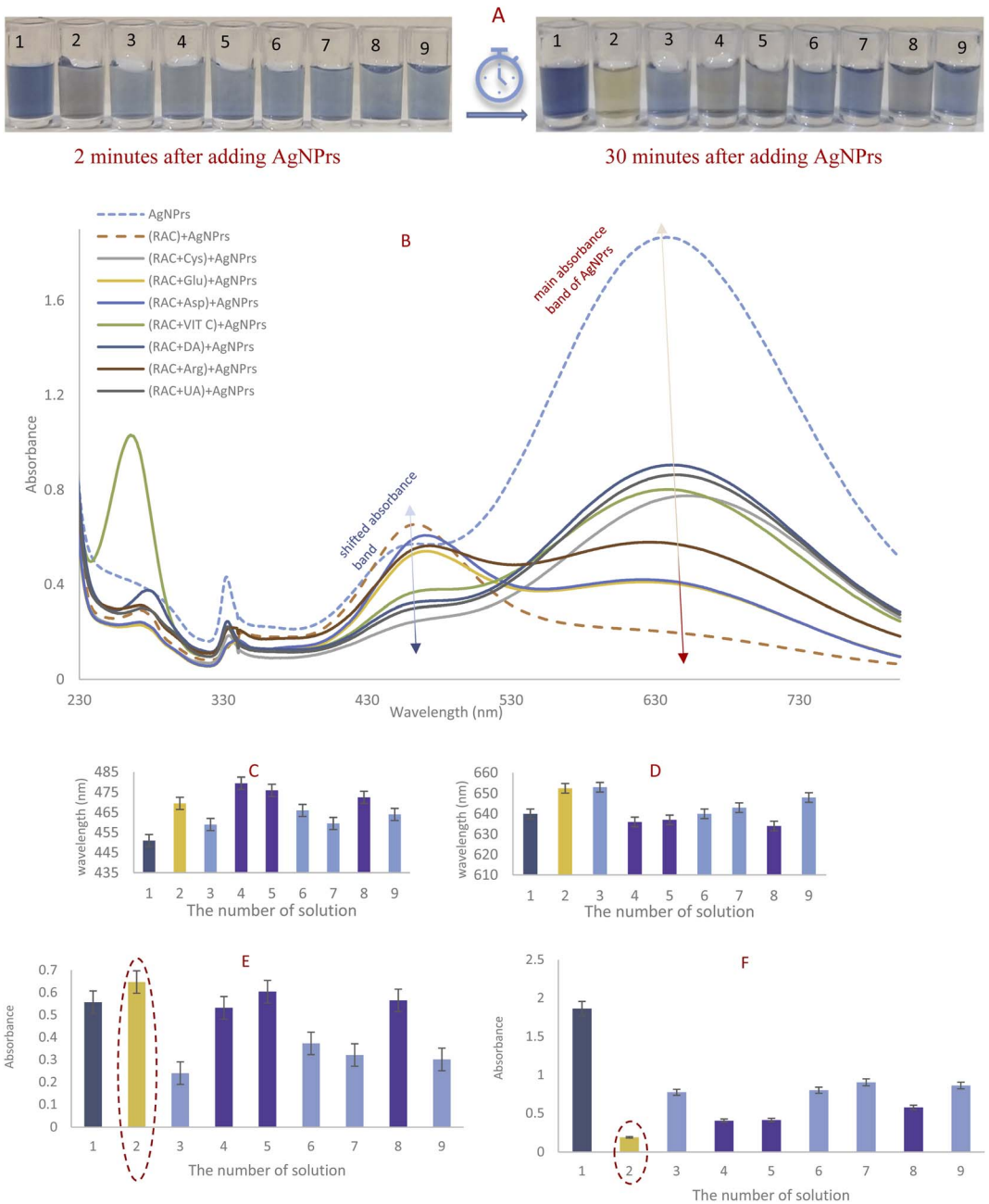

Fig. 4 (A) Photographic images and (B) spectra of (1) AgNPrs, (2) AgNPrs/RAC (1 : 1 v/v ratio), (3) AgNPrs/(RAC + Cys), (4) AgNPrs/(RAC + Glu), (5) AgNPrs/(RAC + Asp), (6) AgNPrs/(RAC + VIT C), (7) AgNPrs/(RAC + DA), (8) AgNPrs/(RAC + Arg), and (9) AgNPrs/(RAC + UA); the ratio of AgNPrs/potential interferent + RAC from no. 3 to no. 9 was 1 : 0.5 : 0.5 v/v/v and the total volume of each solution was 200 μL. (C) The position and (E) the intensity of the absorbance band in the vicinity of 450 nm for each solution in comparison with AgNPrs/RAC. (D) The position and (F) the intensity of the absorbance band in the vicinity of 640 nm for each solution in comparison with AgNPrs/RAC. The concentration of RAC and potential interferent were 0.1 mM.

the first attempt, the microfluidic network was established with 20 seconds of heat and pressure on the fiberglass paper (the instruction is explained in subsection 2.5). The hydrophilic network of prepared microfluidic paper was very permeable towards AgNPrs and RAC. As soon as AgNPrs and RAC were injected, they were absorbed in the paper, so no noticeable color change occurred in the injected areas. In a second attempt, the time of exposure to molten paraffin was increased to 30 seconds consequently, the hydrophilic network changed to a semi-hydrophobic one which was more resistant to absorption of AgNPrs and RAC. As a result, the injected drop of AgNPrs and RAC took almost one hour of reaction time until they either were absorbed into the paper or dried (Fig. 5). This alteration in the preparation of the microfluidic paper made it suitable for AgNPr-based colorimetric systems based on a time/color shift system (see video files†).

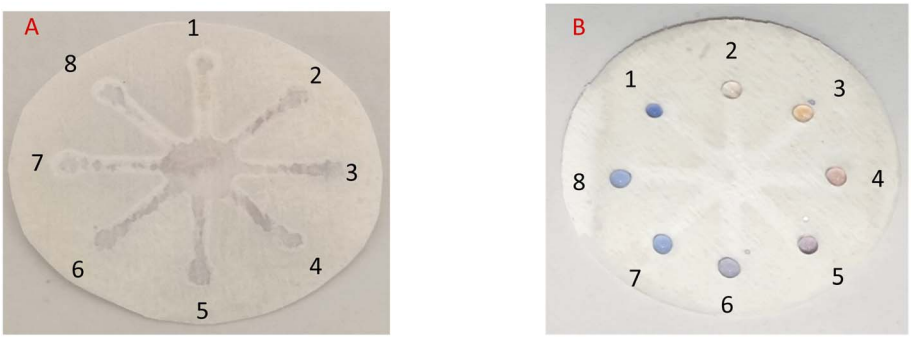

Fig. 5 First-minute photographic images of (A) conventional microfluidic fiberglass paper injected with (1) AgNPrs/5000 μM RAC, (2) AgNPrs/1000 μM RAC, (3) AgNPrs/100 μM RAC, (4) AgNPrs/50 μM RAC, (5) AgNPrs/10 μM RAC, (6) AgNPrs/1 μM RAC, (7) AgNPrs/0.1 μM RAC, and (8) AgNPrs/0.01 μM RAC. (B) Optimized semi-hydrophobic microfluidic fiberglass paper injected with (1) AgNPrs, (2) AgNPrs/10 000 μM RAC, (3) AgNPrs/5000 μM RAC, (4) AgNPrs/1000 μM RAC, (5) AgNPrs/500 μM RAC, (6) AgNPrs/100 μM RAC, (7) AgNPrs/50 μM RAC, and (8) AgNPrs/10 μM RAC. The ratio of AgNPrs/RAC was 1 : 1 v/v and the volume of each was 5 μL.

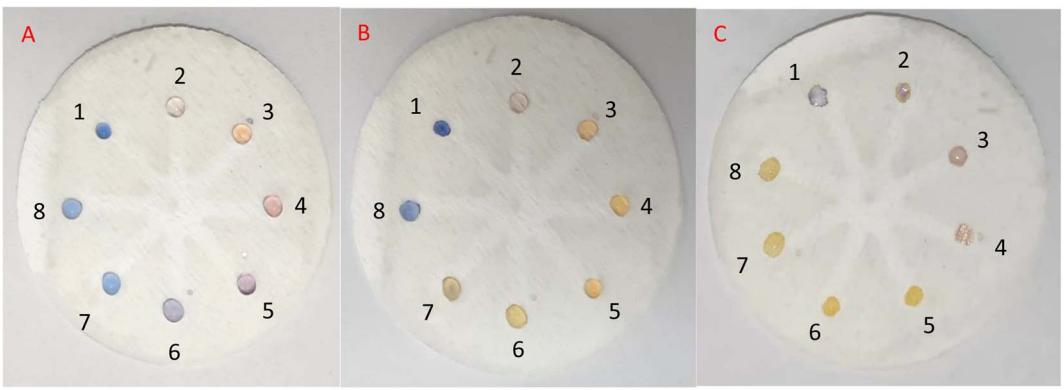

Fig. 6 Photographic images of the fiberglass microfluidic paper-based colorimetric chemosensor after (A) 5 min, (B) 25 min, and (C) 60 min without and with different concentrations of RAC (1) AgNPrs without RAC, (2) AgNPrs, 10 000 μM RAC, (3) AgNPrs, 5000 μM RAC, (4) AgNPrs, 1000 μM RAC, (5) AgNPrs, 500 μM RAC, (6) AgNPrs, 100 μM RAC, (7) AgNPrs, 50 μM RAC, and (8) AgNPrs, 10 μM RAC.

4.5.2. Analytical approach. In a fiberglass microfluidic paper-based colorimetric chemosensor, wells No. 2 to No. 8 were injected with 5 μL of different concentrations of RAC (10 000, 5000, 1000, 500, 100, 50, and 10 μM) followed by the addition of 5 μL of freshly prepared AgNPrs into all wells from No. 1 to No. 8. After 5 min, the color change was obvious in 10 000, 5000, 1000, 500, and 100 μL concentrations of RAC (Fig. 6A). After 25 minutes of reaction time (Fig. 6B), all of the RAC concentrations had experienced a color change to orange except for the concentrations of 10 000 μM of RAC (which had changed to pink) and 10 μM of RAC (which had remained blue). Almost 1 h later, the concentrations of 10 000, 5000, and 1000 μM of RAC were pink in color and the other concentrations were Vegas gold (Fig. 6C). The color for the well without RAC remained blue during this period. Also, the times of color changes and the final color for all of the concentrations were recorded and are displayed in Fig. 7. This bar chart can offer an innovative way of estimating a rough amount of RAC concentration based on a time/color characterization system as the pattern of these bars illustrated a unique pattern for every concentration of RAC (see video files†).

4.5.3. Selectivity analysis. To investigate the effect of the possible intervention of other species in real samples on RAC measurement, the interaction of AgNPrs with seven types of potential interferers, cysteine (Cys), aspartic acid (Asp), arginine (Arg), ascorbic acid (VIT C), dopamine (DA), uric acid (UA) and glucose (Glu), at a concentration of 0.01 M using μPCD were evaluated.

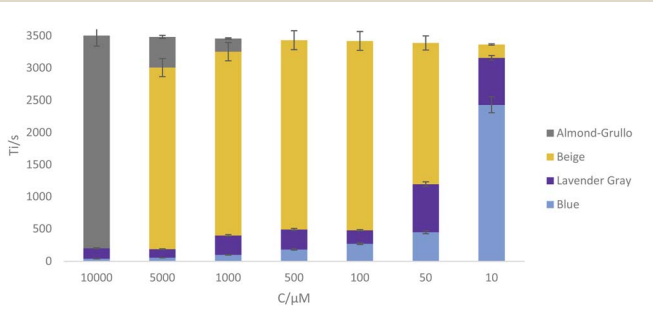

Fig. 7 A graph for comparing the time (*Y*-axis)/color (color shown in bars) characterization of each concentration (*X*-axis) of RAC in μPCD.

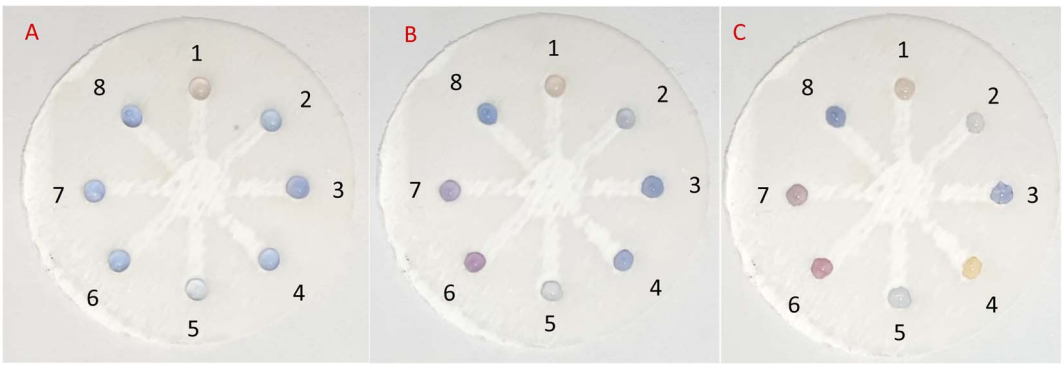

Fig. 8 Photographic images of the fiberglass microfluidic paper-based colorimetric chemosensor (A) after 5 minutes, (B) after 25 minutes, and (C) after an hour: 1. AgNPrs + RAC 0.01 M (1 : 1), 2. AgNPrs + Cys 0.01 M (1 : 1), 3. AgNPrs + Glu 0.01 M (1 : 1), 4. AgNPrs + Asp 0.01 M (1 : 1), 5. AgNPrs + VIT C 0.01 M (1 : 1), 6. AgNPrs + DA 0.01 M (1 : 1), 7. AgNPrs + Arg 0.01 M (1 : 1), and 8. AgNPrs + UA 0.01 M (1 : 1).

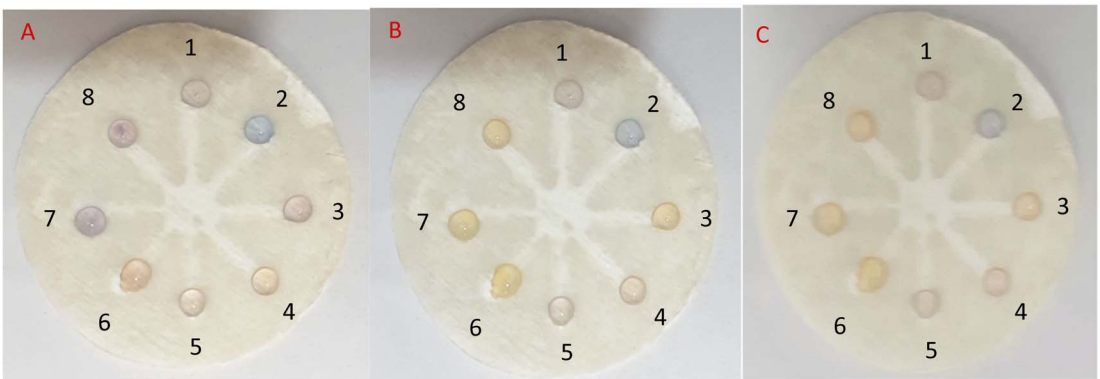

Fig. 9 Photographic images of the fiberglass microfluidic paper-based colorimetric chemosensor (A) after 5 minutes, (B) after 25 minutes, and (C) after an hour: 1. AgNPrs + RAC 0.01 M (1 : 1), 2. AgNPrs + RAC + Cys 0.01 M (1 : 0.5 : 0.5), 3. AgNPrs + RAC + Glu 0.01 M (1 : 0.5 : 0.5), 4. AgNPrs + RAC + Asp 0.01 M (1 : 0.5 : 0.5), 5. AgNPrs + RAC + VIT C 0.01 M (1 : 0.5 : 0.5), 6. AgNPrs + RAC + DA 0.01 M (1 : 0.5 : 0.5), 7. AgNPrs + RAC + Arg 0.01 M (1 : 0.5 : 0.5), and 8. AgNPrs + RAC + UA 0.01 M (1 : 0.5 : 0.5).

In practice, in the initial examination, as shown in Fig. 8, 5 μL of AgNPrs was injected into each well of μPCD from No. 1 to No. 8. Afterward, 5 μL of RAC 0.01 M was added to well No. 1 and potential interferers were added to wells No. 2 to No. 8. After 5 min, the color change of the well containing RAC is quite tangible, while the other wells did not show any noticeable color change. After 25 min, the hue of some of the wells had also changed. Having said that, the pale silver color of the well containing RAC was distinct from the other wells. After one hour, well Nos 2 and 5 containing Cys and VIT C, respectively, had experienced a color shift to neon silver; well Nos 6 and 7 including DA and Arg, respectively, had changed to pink; the color of well No. 4 (Asp) had become beige; while well Nos 3 (Glu) and 8 (UA) remained blue. The obtained results indicate that none of these species can interfere with RAC at the same concentration. Nevertheless, at concentrations <1000 μM of RAC, Asp, by turning the hue of AgNPrs to beige after one hour, can be considered an interferer.

In the subsequent test, 10 μL of RAC was injected into well No. 1, and 5 μL of RAC plus 5 μL of the potential interferer were added to well Nos 2 to 8. After 25 and 60 min of reaction time, the color change became more tangible and stable for each of the wells, as only well No. 2 (RAC + Cys) had not seen any color change (Fig. 9). Also, well Nos 1 (RAC), 4 (RAC + Asp), and 5 (RAC + VIT C) turned to desert sand color, which were similar to each other. The rest of the wells turned tan in color. This result shows that Cys can be a major barrier for the etching effect of RAC on AgNPrs. Therefore, it can be considered an interferer (see video files†).

5. Conclusions

In this innovative study, three different types of silver nanomaterials, namely silver nanoprisms (AgNPrs), Ag-Cit NPs, and silver nanowires (AgNWs), were evaluated for the recognition of RAC. Since AgNPrs showed excellent colorimetric results, they underwent thorough examination. The obtained analytical results for the proposed AgNPr-based colorimetric chemosensor are comparable with others, as this colorimetric system enjoys a broad range of linearity of 0.1–10 000 μM and possesses an LLOQ of 10 nM. Moreover, AgNPrs could successfully detect RAC in a real chicken sample. In the last part of this work, a reported μPCD was optimized for integration with the

colorimetric system. This optimization paved the way for offering an innovative analytical method that is based on the time/color characterization of each concentration of RAC with an LLOQ of 10 μM. The selectivity tests for the devised systems (solution and integrated μPCD) were also appropriate, and the stability of the AgNPrs was confirmed for at least 20 days, which makes the commercialization of the proposed system more achievable. What this study offers, apart from the simple and sensitive colorimetric recognition system for RAC, is an optimized μPCD suitable for solutions like AgNPrs that are readily absorbable by paper and a creative time/color system for obtaining a rough estimation of analyte concentration.

Conflicts of interest

There are no conflicts to declare.

Acknowledgements

We are grateful for financial assistance for this work from the Tabriz University of Medical Sciences' Pharmaceutical Analysis Research Center (Tabriz, Iran).

References

1 A. M. Niño, R. H. Granja, A. C. Wanschel and A. G. Salerno, *Food Control*, 2017, **72**, 289–292.
2 J. Beier and K. M. Beeh, *Int. J. Chronic Obstruct. Pulm. Dis.*, 2011, **6**, 237.
3 Z. Wang, M. Liu, W. Shi, C. Li, S. Zhang and J. Shen, *Food Chem.*, 2015, **183**, 111–114.
4 G. Brambilla, T. Cenci, F. Franconi, R. Galarini, A. Macrı, F. Rondoni, M. Strozzi and A. Loizzo, *Toxicol. Lett.*, 2000, **114**, 47–53.
5 J.-P. Antignac, P. Marchand, B. Le Bizec and F. Andre, *J. Chromatogr. B: Anal. Technol. Biomed. Life Sci.*, 2002, **774**, 59–66.
6 H. Zhang, Q. Zhou, J. Cao and Y. Wang, *Spectrochim. Acta, Part A*, 2013, **116**, 251–257.
7 D. Smith, *J. Anim. Sci.*, 2000, **78**, 2903–2912.
8 A. Stolker and U. T. Brinkman, *J. Chromatogr. A*, 2005, **1067**, 15–53.
9 Z. Li, Y. Wang, W. Kong, C. Li, Z. Wang and Z. Fu, *Biosens. Bioelectron.*, 2013, **39**, 311–314.
10 V. Amelin, D. Korolev and A. Tret'Yakov, *J. Anal. Chem.*, 2015, **70**, 419–423.
11 V. Gressler, A. R. Franzen, G. J. de Lima, F. C. Tavernari, O. A. Dalla Costa and V. Feddern, *J. Chromatogr. B: Anal. Technol. Biomed. Life Sci.*, 2016, **1015**, 192–200.
12 C. T. Elliott, C. S. Thompson, S. R. Crooks, G. A. Baxter, C. J. Arts, M. J. van Baak and E. R. Verheij, *Analyst*, 1998, **123**, 1103–1107.
13 W. L. Shelver and D. J. Smith, *J. Immunoassay*, 2000, **21**, 1–23.
14 S. Han, T. Zhou, B. Yin and P. He, *Anal. Chim. Acta*, 2016, **927**, 64–71.
15 W. L. Shelver and D. J. Smith, *J. Agric. Food Chem.*, 2003, **51**, 3715–3721.
16 Q. Wei, Q. Wang, H. Wang, H. Gu, Q. Zhang, X. Gao and B. Qi, *Mater. Lett.*, 2015, **147**, 58–60.
17 Y. Zhou, P. Wang, X. Su, H. Zhao and Y. He, *Microchim. Acta*, 2014, **181**, 1973–1979.
18 H. K. Kordasht, A. Saadati and M. Hasanzadeh, *Food Chem.*, 2022, **373**, 131411.
19 Y. Sun, T. Fu, S. Chen, Z. Wu, Y. Guo, D. Pan and N. Gan, *J. Sci. Food Agric.*, 2019, **99**, 2818–2825.
20 Y. Luo, X. Liu, H. Gao H, Y. Li, J. Xu, F. Shen and C. Sun, *J. Nanosci. Nanotechnol.*, 2016, **16**, 548–554.
21 Y. Zhou, P. Wang, X. Su, H. Zhao and Y. He, *Talanta*, 2013, **112**, 20–25.
22 X. Hu, J. Du, J. Pan, F. Wang, D. Gong and G. Zhang, *Food Addit. Contam., Part A*, 2019, **36**, 35–45.
23 T. Simon, M. Shellaiah, P. Steffi, K. W. Sun and F.-H. Ko, *Anal. Chim. Acta*, 2018, **1023**, 96–104.
24 X. Duan, Z. Bai, X. Shao, J. Xu, N. Yan, J. Shi and X. Wang, *Materials*, 2018, **11**, 674.
25 G. M. Fernandes, W. R. Silva, D. N. Barreto, R. S. Lamarca, P. C. F. L. Gomes, J. F. da S Petruci and A. D. Batista, *Anal. Chim. Acta*, 2020, **1135**, 187–203.
26 X. Lu, X. Dong, K. Zhang, X. Han, X. Fang and Y. Zhang, *Analyst*, 2013, **138**, 642–650.
27 K. Caswell, C. M. Bender and C. J. Murphy, *Nano Lett.*, 2003, **3**, 667–669.
28 K. L. Kelly, E. Coronado, L. L. Zhao and G. C. Schatz, *J. Phys. Chem. B*, 2003, **107**, 668–677.
29 E. Oliveira, C. Núñez, H. M. Santos, J. Fernández-Lodeiro, A. Fernández-Lodeiro, J. L. Capelo and C. Lodeiro, *Sens. Actuators, B*, 2015, **212**, 297–328.
30 C. Liu, Q. Pang, T. Wu, W. Qi, W. Fu and Y. Wang, *J. Anal. Testing*, 2021, **5**, 210–216.
31 T. Lou, Z. Chen, Y. Wang and L. Chen, *ACS Appl. Mater. Interfaces*, 2011, **3**, 1568–1573.
32 M. Amjadi, T. Hallaj and R. Salari, *Sens. Actuators, B*, 2018, **273**, 1307–1312.
33 D.-K. Lim, I.-J. Kim and J.-M. Nam, *Chem. Commun.*, 2008, 5312–5314.
34 G. S. Métraux and C. A. Mirkin, *Adv. Mater.*, 2005, **17**, 412–415.
35 J. E. Millstone, S. J. Hurst, G. S. Métraux, J. I. Cutler and C. A. Mirkin, *Small*, 2009, **5**, 646–664.
36 X. Jiang and A. Yu, *Langmuir*, 2008, **24**, 4300–4309.
37 N. Cathcart, A. J. Frank and V. Kitaev, *Chem. Commun.*, 2009, 7170–7172.
38 Q. Zhang, N. Li, J. Goebl, Z. Lu and Y. Yin, *J. Am. Chem. Soc.*, 2011, **133**, 18931–18939.
39 B. Malile and J. I. Chen, *J. Am. Chem. Soc.*, 2013, **135**, 16042–16045.
40 K. Tan, G. Yang, H. Chen, P. Shen, Y. Huang and Y. Xia, *Biosens. Bioelectron.*, 2014, **59**, 227–232.
41 N. Chen, Y. Zhang, H. Liu, X. Wu, Y. Li, L. Miao, Z. Shen and A. Wu, *ACS Sens.*, 2016, **1**, 521–527.
42 Y. Zhou, W. Huang and Y. He, *Sens. Actuators, B*, 2018, **270**, 187–191.
43 Y. Guo, J. Wu, J. Li and H. Ju, *Biosens. Bioelectron.*, 2016, **78**, 267–273.

44 Y. Wang, P. Zhang, X. Mao, W. Fu and C. Liu, *Sens. Actuators, B*, 2016, **231**, 95–101.
45 L. Y. Yeo, H. C. Chang, P. P. Chan and J. R. Friend, *Small*, 2011, **7**, 12–48.
46 G. Luka, A. Ahmadi, H. Najjaran, E. Alocilja, M. DeRosa, K. Wolthers, A. Malki, H. Aziz, A. Althani and M. Hoorfar, *Sensors*, 2015, **15**, 30011–30031.
47 P. de Tarso Garcia, T. M. G. Cardoso, C. D. Garcia, E. Carrilho and W. K. T. Coltro, *RSC Adv.*, 2014, **4**, 37637–37644.
48 *The free download of Instant Eyedropper*, **https://www.instant-eyedropper.com**, (accessed August 2022).
49 *The conversion of RGBA code to color*, **https://www.colorxs.com**, (accessed August 2022).
50 Z. Sun, Y. Sun, M. Yang, H. Jin and R. Gui, *Nanoscale*, 2021, **13**, 13014–13023.
51 D. Aherne, D. M. Ledwith, M. Gara and J. M. Kelly, *Adv. Funct. Mater.*, 2008, **18**, 2005–2016.
52 X. Fang, H. Ren, H. Zhao and Z. Li, *Microchim. Acta*, 2017, **184**, 415–421.
53 A. Seidavi, H. Zaker-Esteghamati and C. Scanes, *World's Poult. Sci. J.*, 2019, **75**, 55–68.
54 S. Han, T. Zhou, B. Yin and P. He, *Microchim. Acta*, 2018, **185**, 1–8.
55 W. Wang, Y. Zhang, J. Wang, X. Shi and J. Ye, *Meat Sci.*, 2010, **85**, 302–305.
56 L. He, Y. Su, Z. Zeng, Y. Liu and X. Huang, *Anim. Feed Sci. Technol.*, 2007, **132**, 316–323.
57 A. Mirzaie, M. Hasanzadeh and A. Jouyban, *Int. J. Biol. Macromol.*, 2019, **123**, 1091–1105.
58 M. P. Turberg, J. M. Rodewald and M. R. Coleman, *J. Chromatogr. B: Biomed. Sci. Appl.*, 1996, **675**, 279–285.